SUPPLEMENTARY MATERIAL

Photooxidation of nucleic acids on metal oxides: physico-chemical and astrobiological perspectives.

Ilya A. Shkrob,* [1] Timothy M. Marin, [1,2] Amitava Adhikary, [3] and Michael D. Sevilla [3]

[1] *Chemical Sciences and Engineering Division, Argonne National Laboratory, 9700 S. Cass Ave, Argonne, IL 60439*

[2] *Chemistry Department, Benedictine University, 5700 College Road, Lisle, IL 60532*

[3] *Department of Chemistry, Oakland University, Rochester, Michigan 48309*

shkrob@anl.gov tel. (630) 252-9516

Table 1S.

Calculated magnetic parameters for allyl-T/dT and allyl-C/dC radicals (DFT method B3LYP/6-31+G).** [a]

structure	a_{iso}, G	$\mathbf{B}_{aa}$, G	$\mathbf{B}_{bb}$, G	$\mathbf{B}_{cc}$, G	α_X, ^{o}	β_Y, ^{o}	γ_Z, ^{o}	$(g_{\perp,\parallel}-2)$, x 10^4 exp. [c]
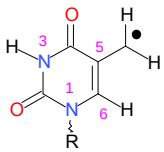 allyl-T/dT Figure 4S	C^1H_2 -16.9 C^1H_2 -15.8 $^1H(6)$ -12.3 $^{13}CH_2$ 27.1	-9.2 -8.2 -5.7 -17.0	0 -0.4 -0.7 -16.5	9.2 8.6 6.4 33.6	90 -90 -90 -180	0	-119.7 0 10.8 54.6	(30,23)
allyl-T/dT 30° out of plane C(6)-H Figure 8S	C^1H_2 -14.3 C^1H_2 -15.2 $^1H(6)$ -9.4	-7.1 -8.3 -6.5	-0.6 -0.1 -0.9	7.7 8.4 7.4	2 -2 22.3	0 61 13.4	0	-
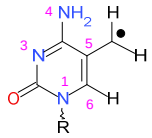 allyl-C/dC Figure 6S	C^1H_2 -16.8 C^1H_2 -16.2 $^1H(6)$ -9.7 $^{14}N(1)$ 1.1	-9.5 -8.5 -4.3	0.1 -0.3 -0.8	9.3 8.8 5.1	90 -90 -90	0	-118 0 8.8	(30,24)

[a] The g-tensor was estimated from numerical simulations of experimental EPR spectra.

[b] Principal components of the anisotropic hfcc tensor ($\mathbf{B}_{aa}$, $\mathbf{B}_{bb}$, $\mathbf{B}_{cc}$): axis *b* (axis z of the molecular frame) is perpendicular to the molecule, axis *c* is (approximately) directed

along the bonds; a_{iso} is the isotropic (Fermi) constant. Only hfcc constants > 1 G are given. Euler angles (α_X,0,γ_Z) for rotation of the molecular frame (XYZ convention) to the principal axes (*a*,*b*,*c*) are also given.

Figure captions (Figure 1S to 14S).

Figure 1S.
Simulated powder EPR spectra of h_8 and d_8 isotopomers of purine bases using hfcc tensors calculated using DFT (isotropic g-tensors).

Figure 2S.
Temperature dependence for GTP on TiO_2.

Figure 3S.
Expanded version of Figure 3 in the main text. A comparison of EPR spectra from cytidine (bold line), 5',5''-d_2-cytidine (thin line) and cytidine-5'-monophosphate (dashed line) on photoirradiated aqueous anatase nanoparticles at 50 K (X=H, Y=OH). The collapsed line (indicated by arrows) is from 5',5''-d_2-$^{\bullet}$C(5) H atom loss ribose radical. The two upper traces are comparisons of X=Me (solid lines) and X=H cytidine (Y=OH) and 2'-deoxycytidine (Y=H) (dashed lines). The features indicated by open circles are from allyl-C/dC radical (see Figure 11S).

Figure 4S.
At the top: simulated EPR spectra from a planar allyl-T/dT radical (Scheme 4 and the inset). The fit parameters are given in Table 1S; the Gaussian linewidth in this simulation was 3.4 G. The dashed line is the EPR spectrum of the allyl-dT radicals observed in γ-irradiated frozen solution of $(dT)_6$ in 8M $NaClO_4/D_2O$ glass. []

Figure 5S.
Angular dependence (H-$^{\bullet}$C-C(5)-C(6) torsion angle) of isotropic hfcc's for carbon-13 and methylene protons and H(6) in allyl-T/dT radical (DFT calculation). At the top of the plot, angular dependence of the conformation energy and the trial angle distribution with the mean angle of 17.5^{o} (corresponding to Boltzmann distribution at 2000 K) are given. The C(5)$CH_2^{\bullet}$ fragment and uracil ring were planar; all other degrees of freedom were optimized.

Figure 6S.
Simulated EPR spectra of allyl-dT radical (a) d_2- and h_2- and (b) $^{13}CH_2$ isotopomers for constrained rotation of the methylene group (that is, the spectra are weighed ensemble averages for frozen radical conformers). The inset in the plot gives the corresponding mean angles for trial angle distributions.

Figure 7S.
Angular dependence (out of plane C(6)-H angle) of H(6) and methylene proton a_{iso} and $\mathbf{B}_{cc}$ for allyl-T/dT radicals (DFT calculation). As the bending angle increases, the absolute coupling constants for methylene and H(6) protons both decrease, whereas the dipolar coupling decreases for the methylene protons and increases for H(6). The uracil residue was planar and all other degrees of freedom were optimized. The energy of this bending is ~0.2 eV for an angle of 30°.

Figure 8S.
Simulated EPR spectra for planar (solid line) and bent, 30° out-of-plane C(6)-H (dashed line) allyl-T radicals. The hfcc parameters are given in Table 1S; isotropic g-tensor was assumed and the Gaussian linewidth was 5 G. It is seen that the effect of out-of-plane bend in the allyl is (i) decreasing the *aa*' spacing between the outer lines by ~6 G and (ii) decreasing the relative weight of the singlet at the center of the spectrum. Both of these changes improve the correspondence between the experimental and simulated spectra shown in Figure 4S.

Figure 9S.
Comparison of experimental spectra (solid lines) for isotopomers of dT on TiO_2 and DFT simulations. Trace (i) is for a planar allyl-T/dT radical simulated with parameters similar to those in Table 1S but with the long axes of the **B** tensors aligned with the corresponding C-H bonds and the two methylene protons magnetically equivalent; the spectrum was convoluted with a Voigt linewidth function (a 1:1 Lorentzian-Gaussian with full width at half maximum of 5 G). The dashed traces (ii) are obtained by ensemble averaging of allyl-dT conformers with the mean H-$^{\bullet}$C-C(5)-C(6) torsion angle of 17.5^o (the angular distribution is shown at the top of Figure 5S). In the latter simulation, the g-tensor was assumed to be isotropic for the entire ensemble.

Figure 10S.
Temperature dependence for 5',5''-d_2-dT on TiO_2.

Figure 11S.
Comparison of EPR spectra from cytidine (dash dot line) and 5-methylcytidine (solid line) on photoirradiated aqueous anatase nanoparticles. The dashed trace above is the scaled difference trace; the solid line is the simulated spectrum for allyl-dC (or allyl-C) radical shown in the inset. The vertical lines highlight the features of this radical in the experimental spectrum. Simulation parameters are given in Table 1S.

Figure 12S.
Photooxidation of d_3-methylated 2'-deoxythymidine (solid line) and thymine (dash-dot line) on aqueous anatase and goethite at 50 K. The spin centers in the matrix are indicated with open circles.

Figure 13S.
Photooxidation of h_8 and d_8 isotopomers of GMP and dGMP on goethite at 50 K. The dashed lines (of the same color) are for anatase. The features indicated by open circles are from the spin centers in the oxide matrix.

Figure 14S.
As Figure 13S, for hematite.

Figure 1S.

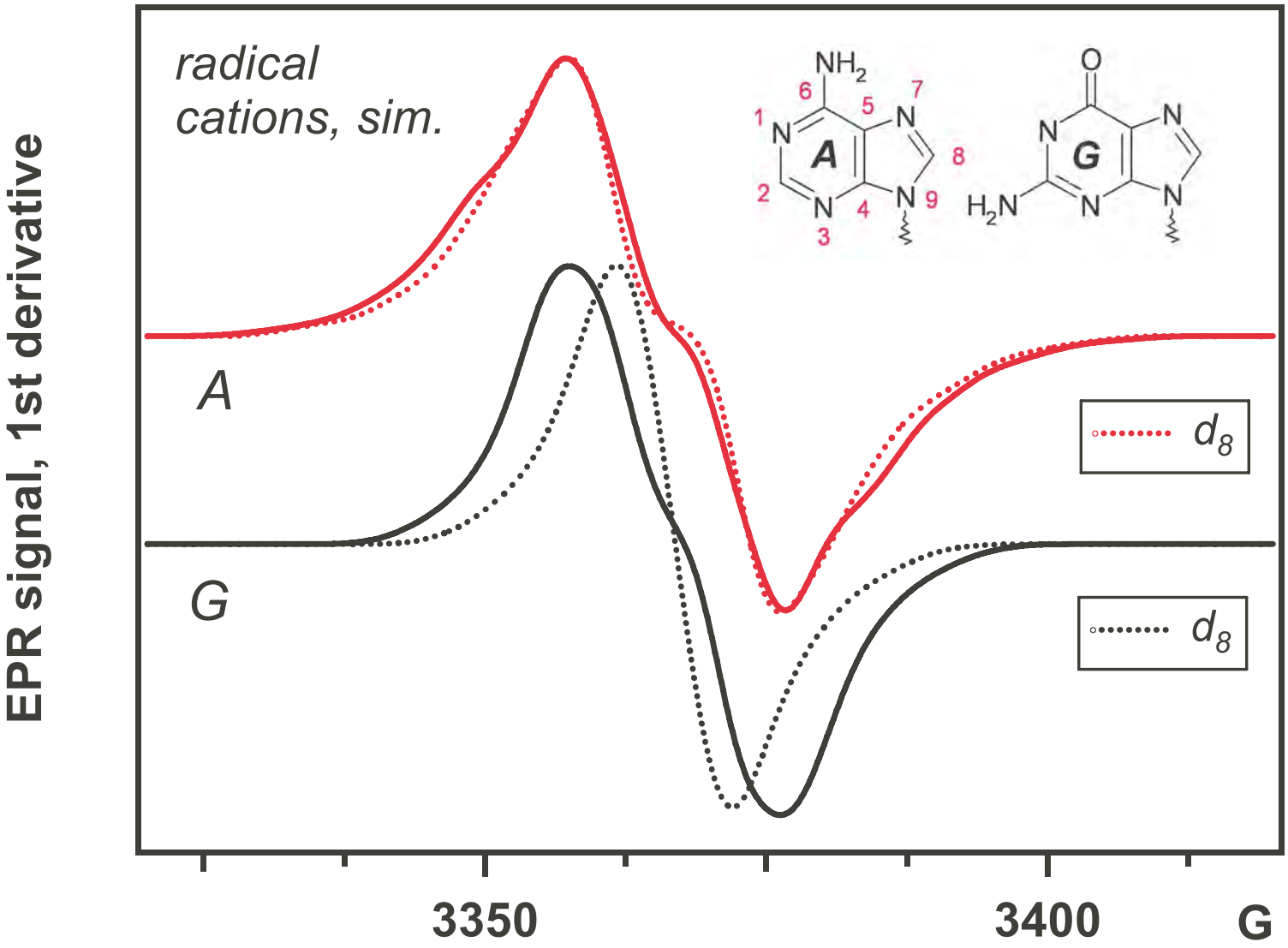
radical
cations, sim.
A
G
d8
d8
EPR signal, 1st derivative
3350
3400
G

Figure 2S.

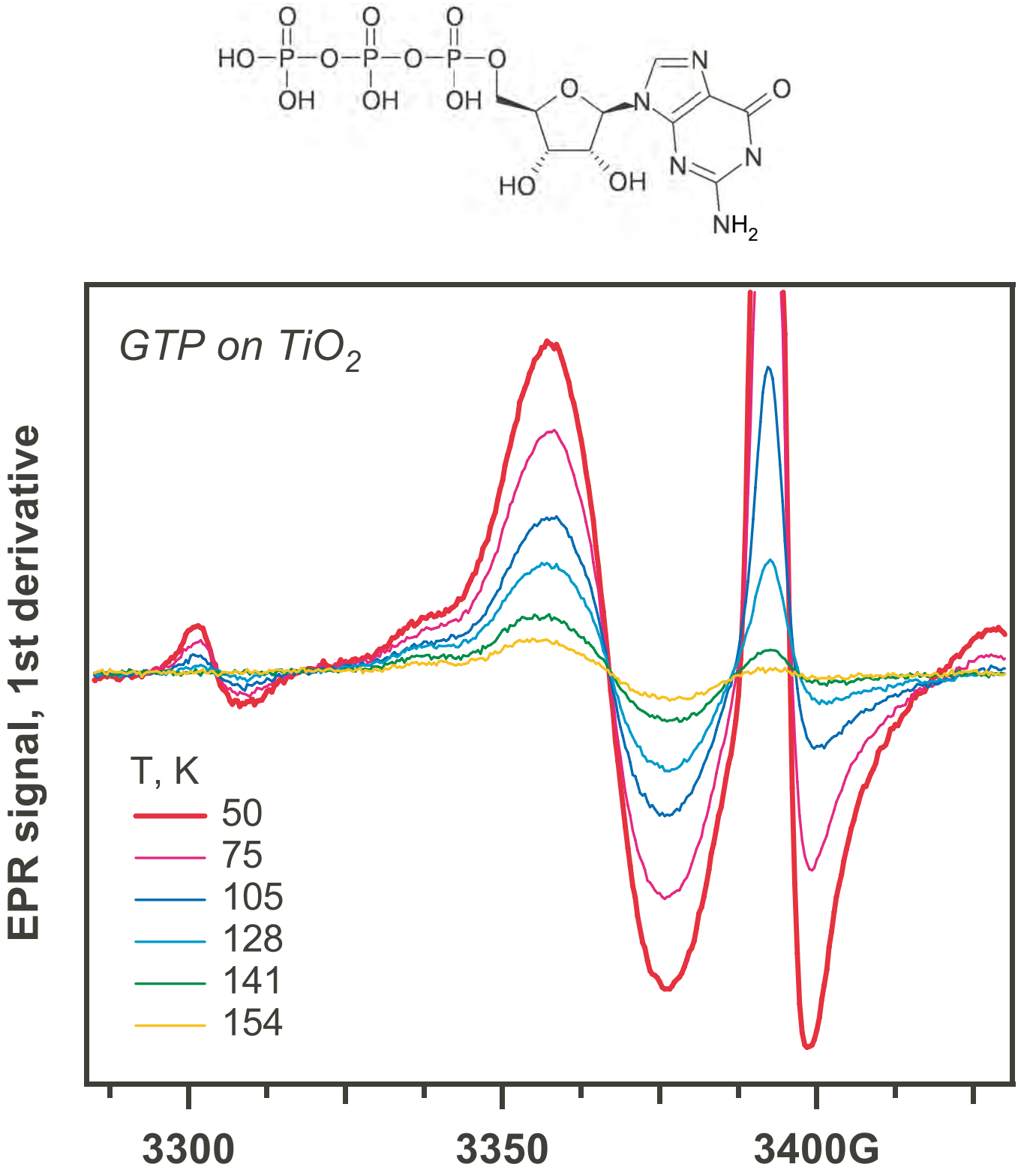

Shkrob et al.

Figure 3S.

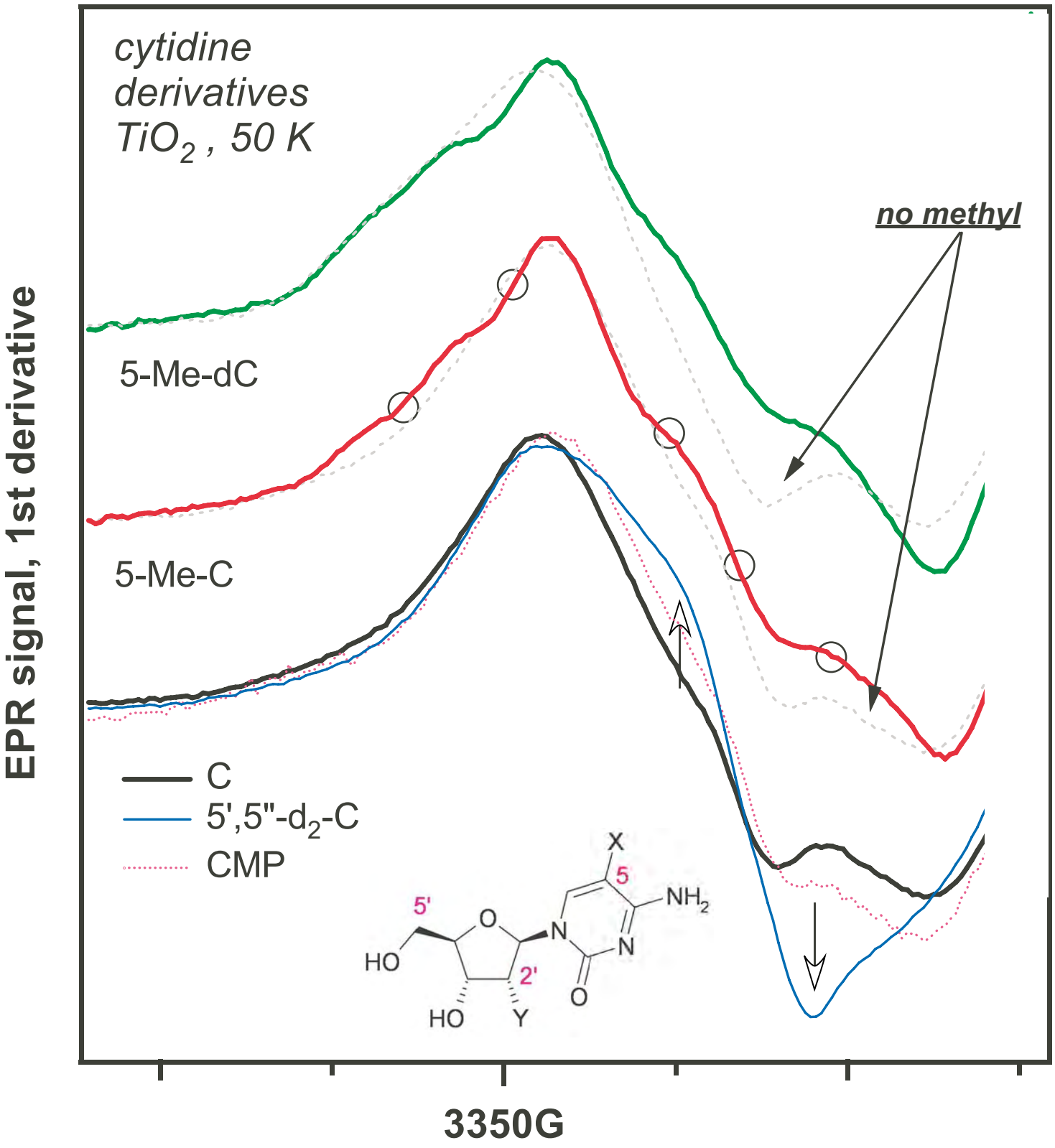
cytidine
derivatives
TiO2 , 50 K
no methyl
5-Me-dC
5-Me-C
C
5',5''-d2-C
CMP
EPR signal, 1st derivative
3350G
X
5
NH2
5'
O
N
N
HO
2'
HO
Y
O

Figure 4S.

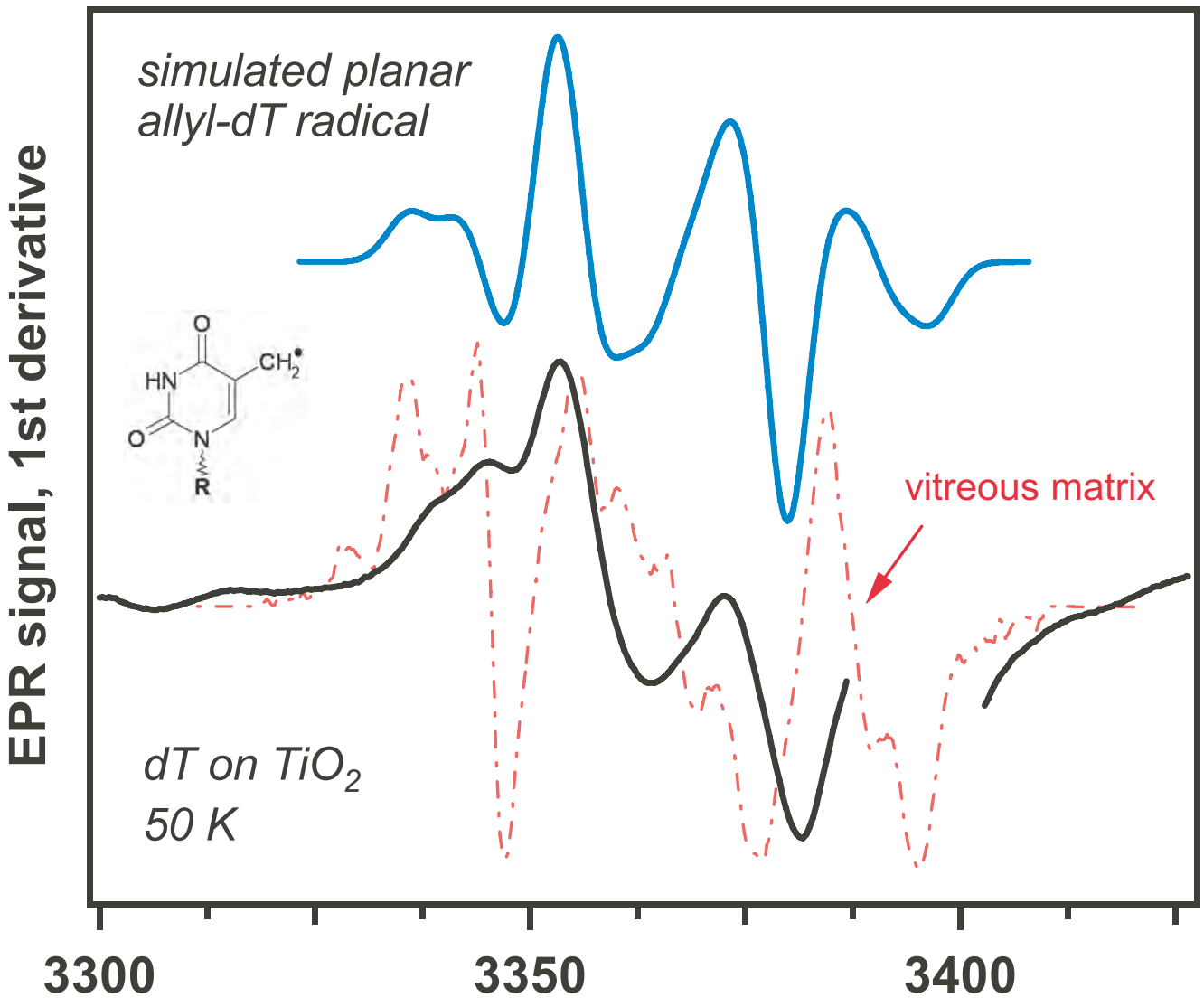
simulated planar
allyl-dT radical
vitreous matrix
dT on TiO2
50 K
EPR signal, 1st derivative
3300
3350
3400

Figure 5S.

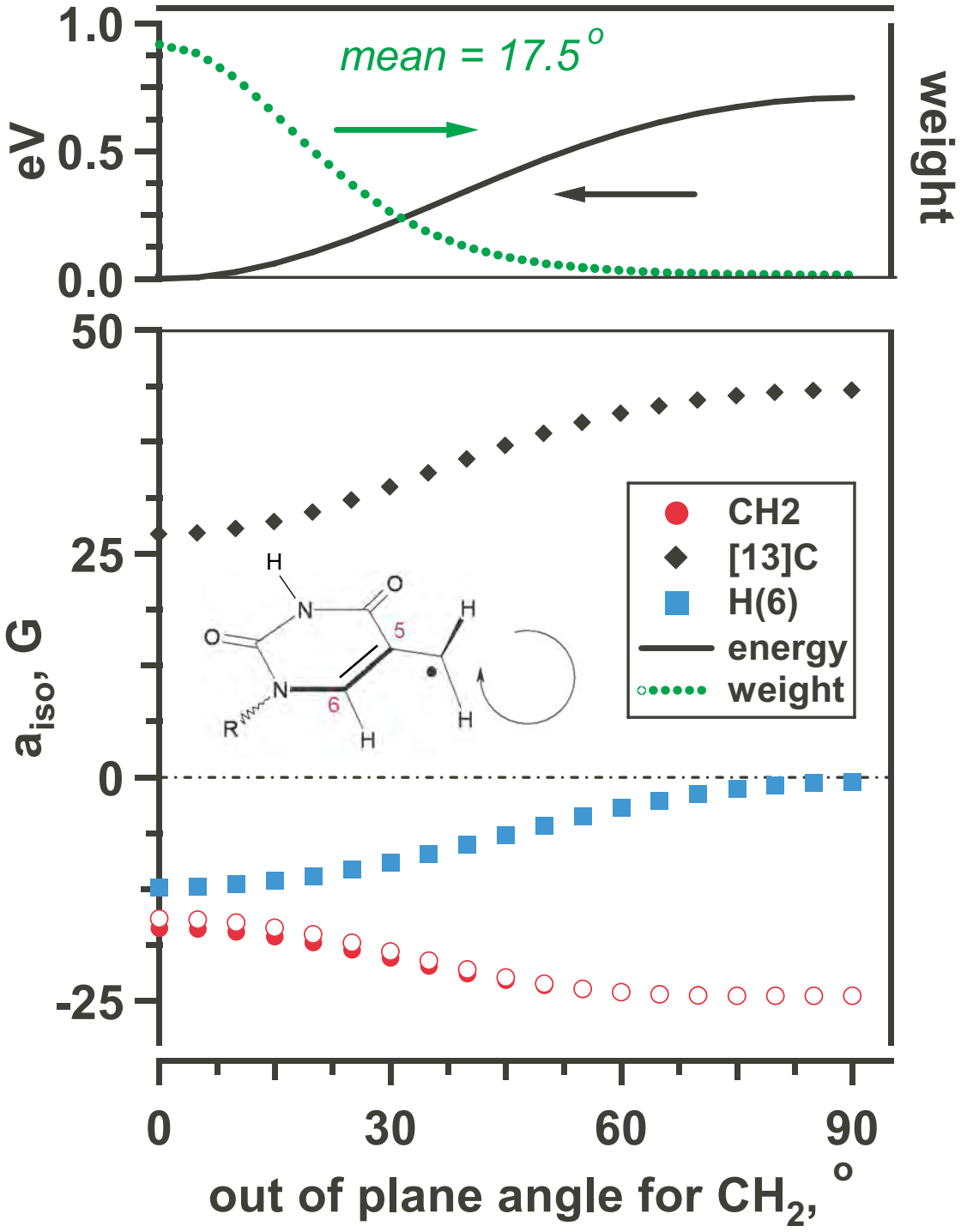
1.0
0.5
0.0
eV
mean = 17.5°
weight
50
25
0
-25
a_{iso}, G
CH2
[13]C
H(6)
energy
weight
0
30
60
90
out of plane angle for CH_2, °

Figure 6S.

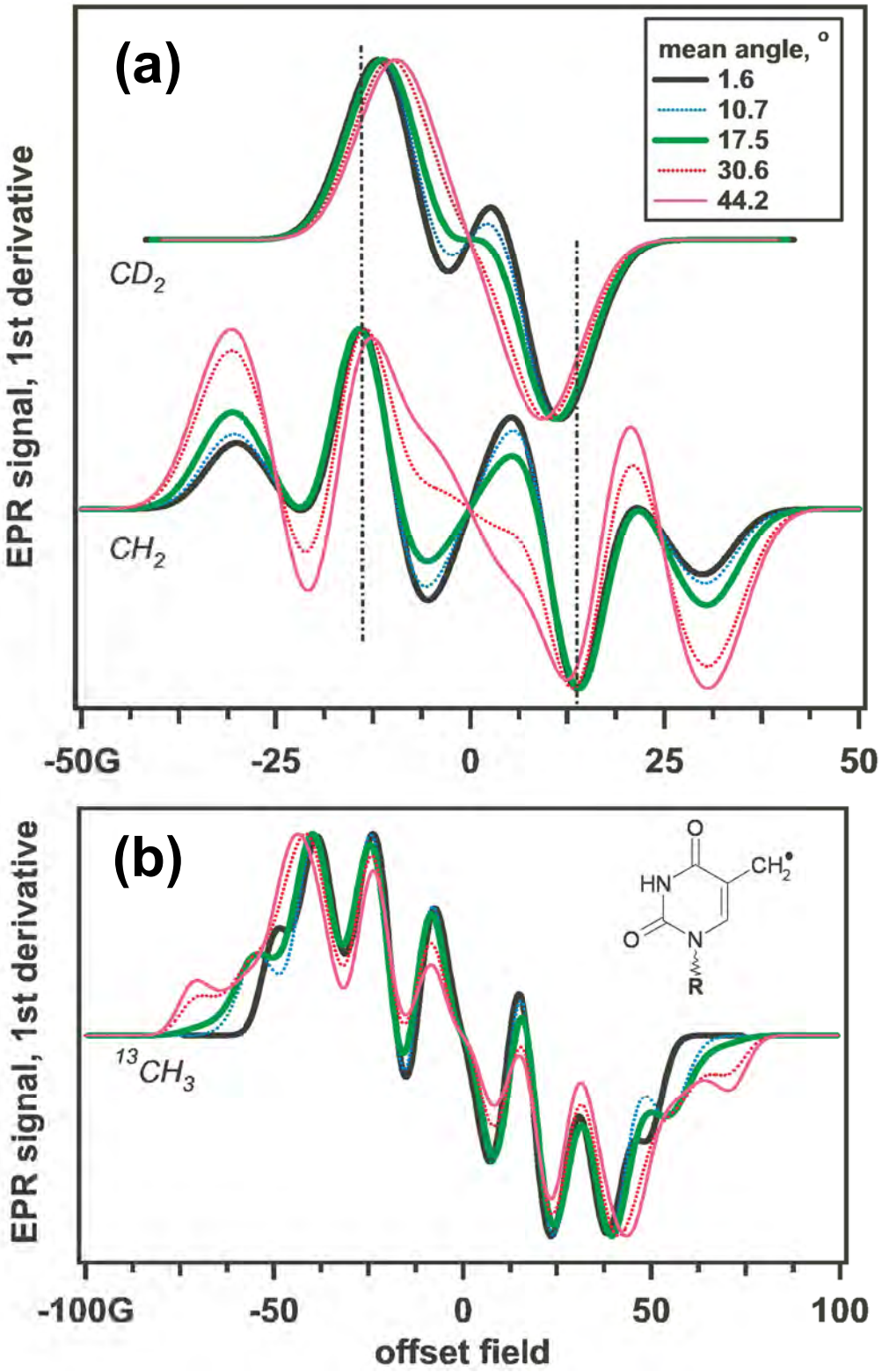
(a)
mean angle, °
1.6
10.7
17.5
30.6
44.2
CD_2
CH_2
EPR signal, 1st derivative
-50G
-25
0
25
50
(b)
$^{13}CH_3$
HN
O
N
R
$CH_2^•$
EPR signal, 1st derivative
-100G
-50
0
50
100
offset field

Figure 7S.

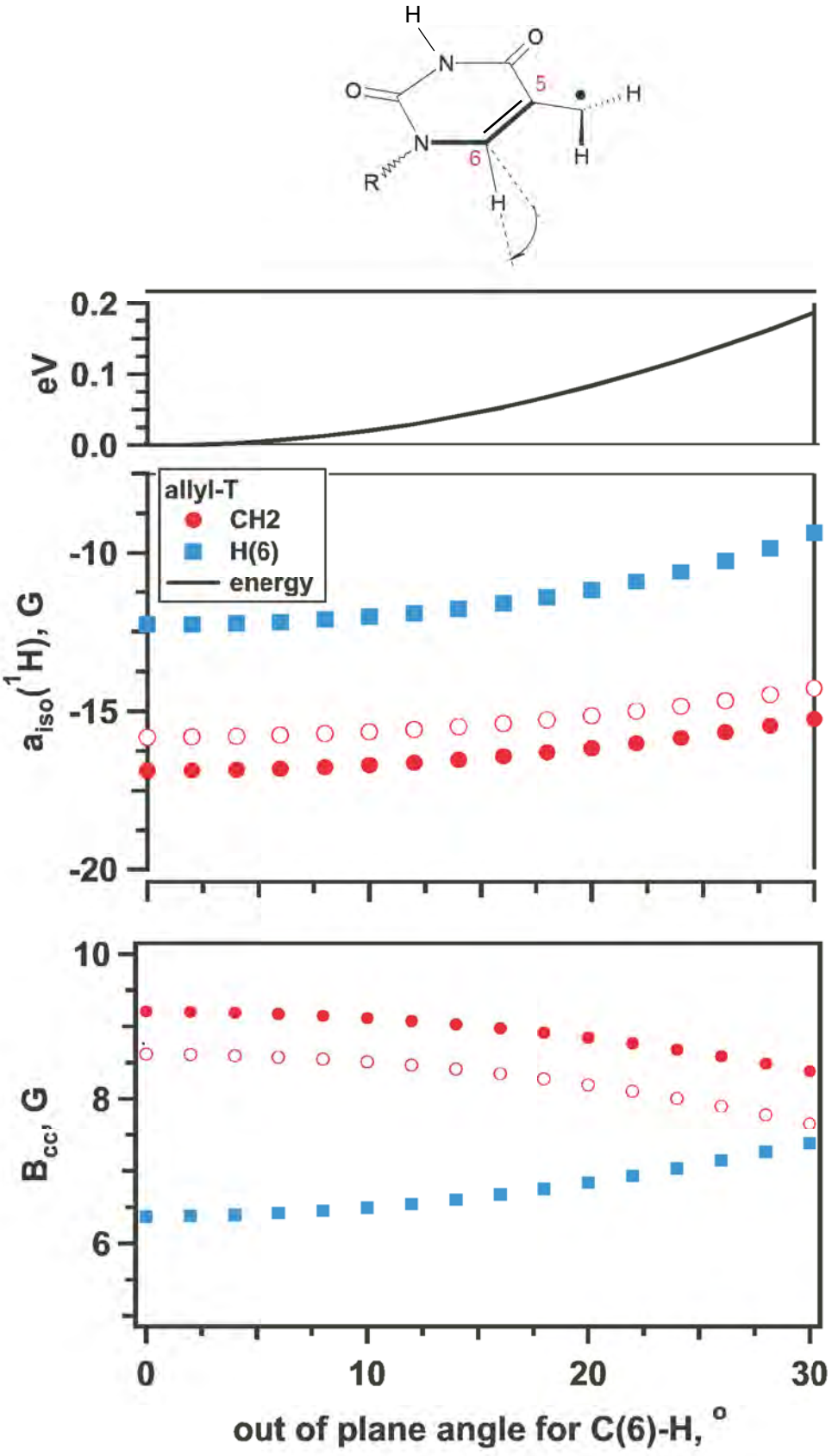

Shkrob et al.

Figure 8S.

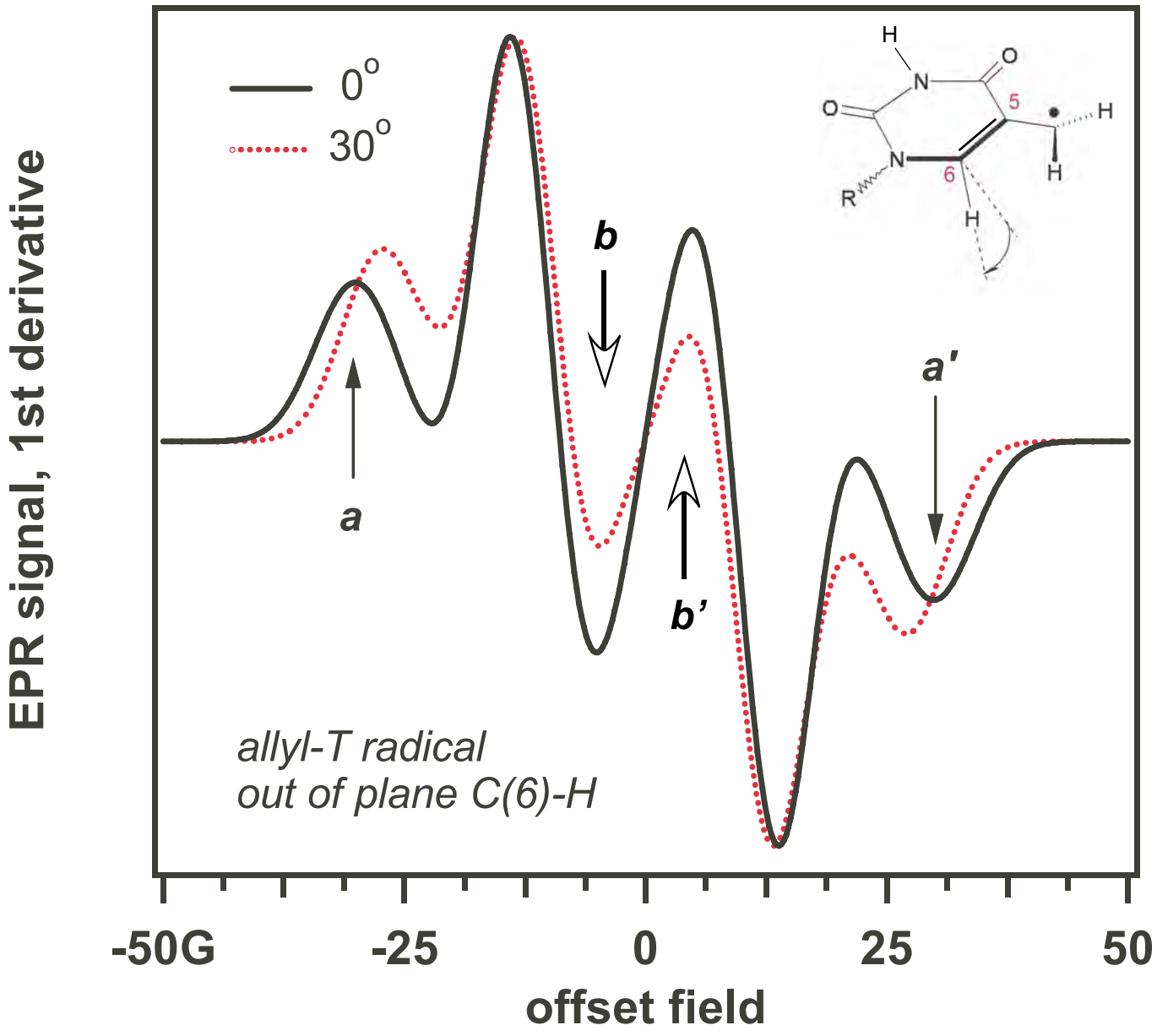
0°
30°
b
a
b'
a'
allyl-T radical
out of plane C(6)-H
EPR signal, 1st derivative
-50G
-25
0
25
50
offset field

Figure 9S.

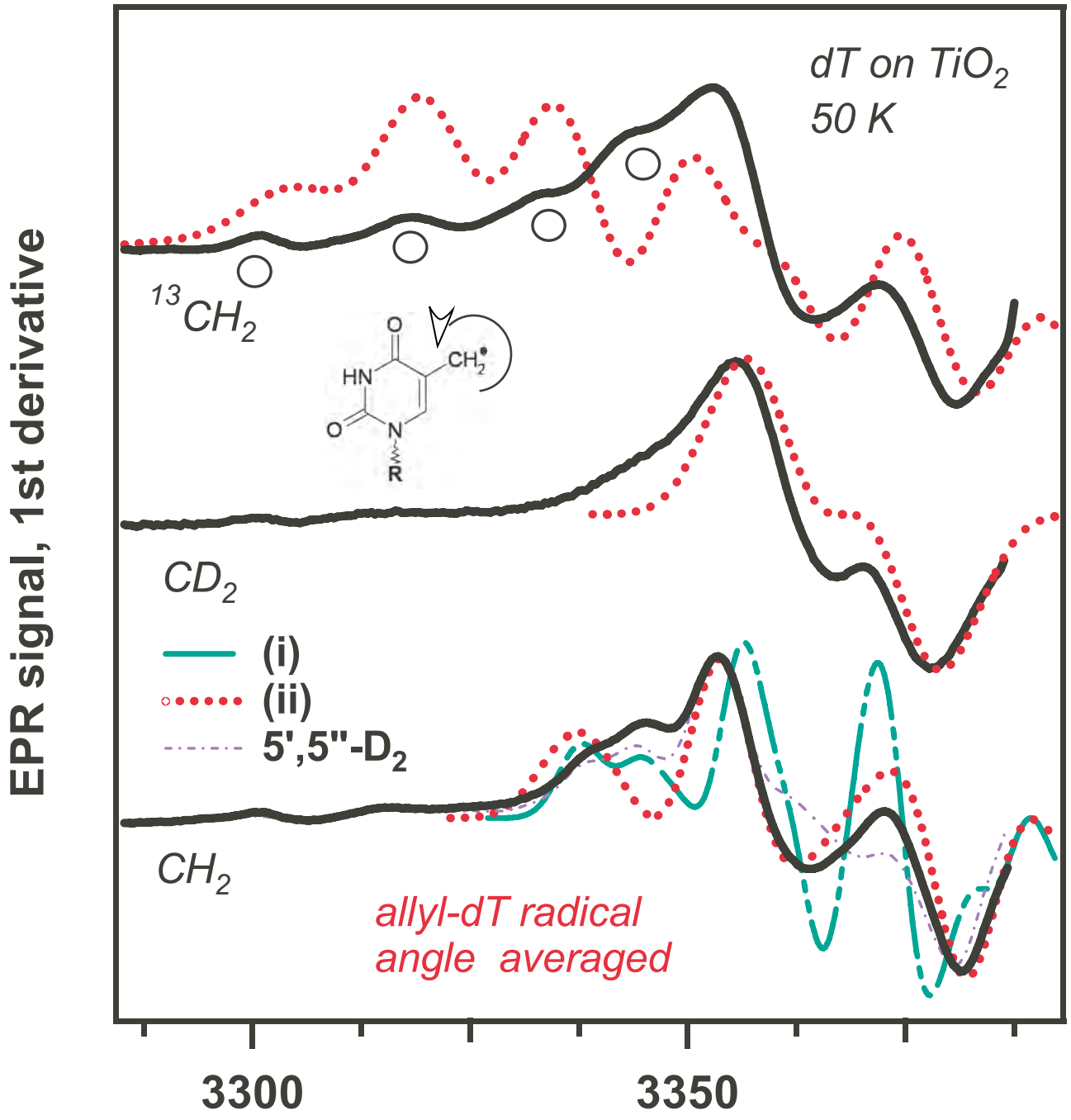
dT on TiO2
50 K
13CH2
CD2
CH2
(i)
(ii)
5',5"-D2
allyl-dT radical
angle averaged
EPR signal, 1st derivative
3300
3350

Figure 10S.

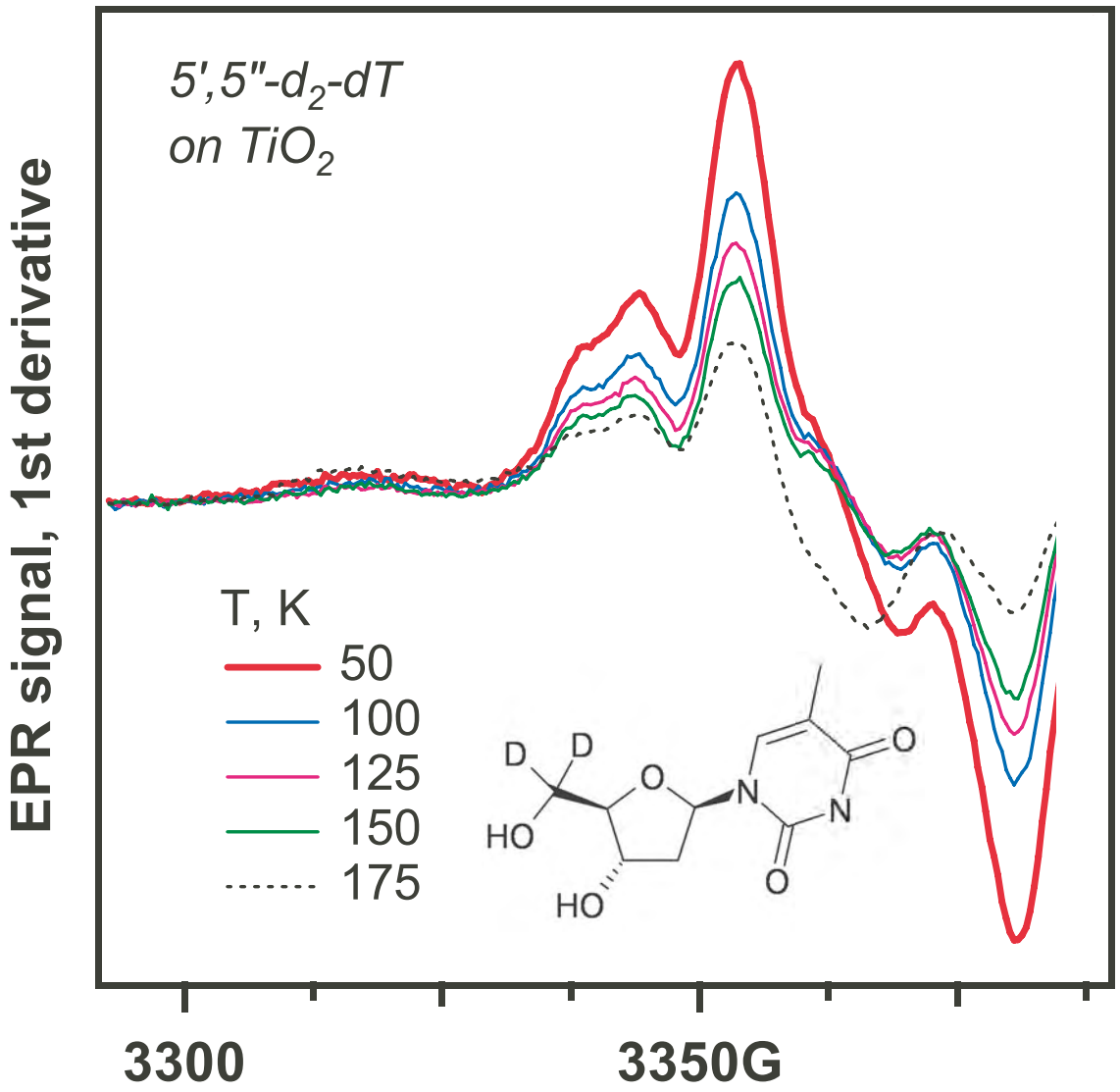
5',5''-d2-dT
on TiO2
EPR signal, 1st derivative
T, K
50
100
125
150
175
D
D
HO
O
HO
N
N
O
O
3300
3350G

Figure 11S.

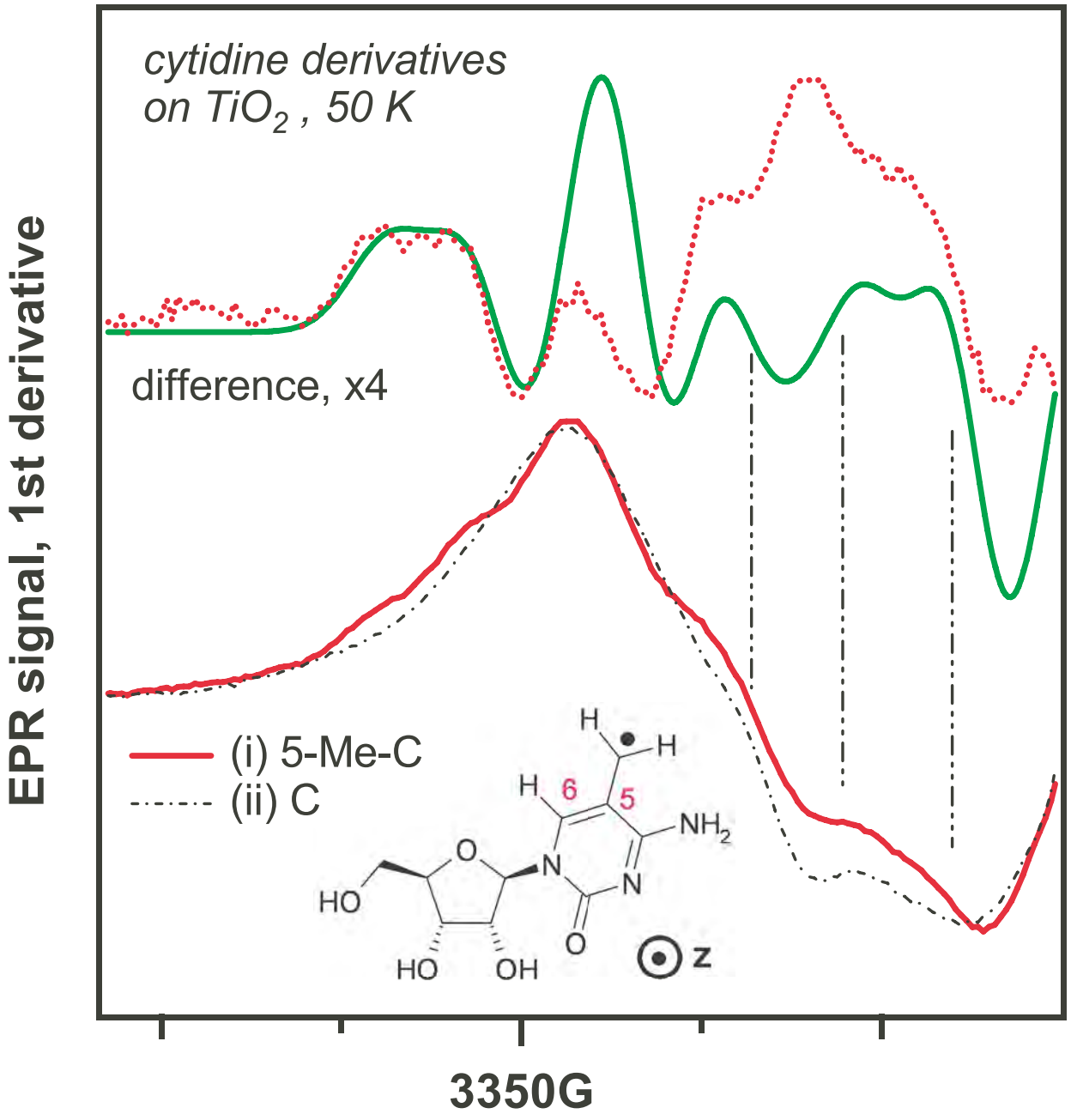
cytidine derivatives
on TiO2 , 50 K
difference, x4
(i) 5-Me-C
(ii) C
EPR signal, 1st derivative
3350G
H
H
H
6
5
NH2
O
N
N
HO
O
HO
OH
z

Figure 12S.

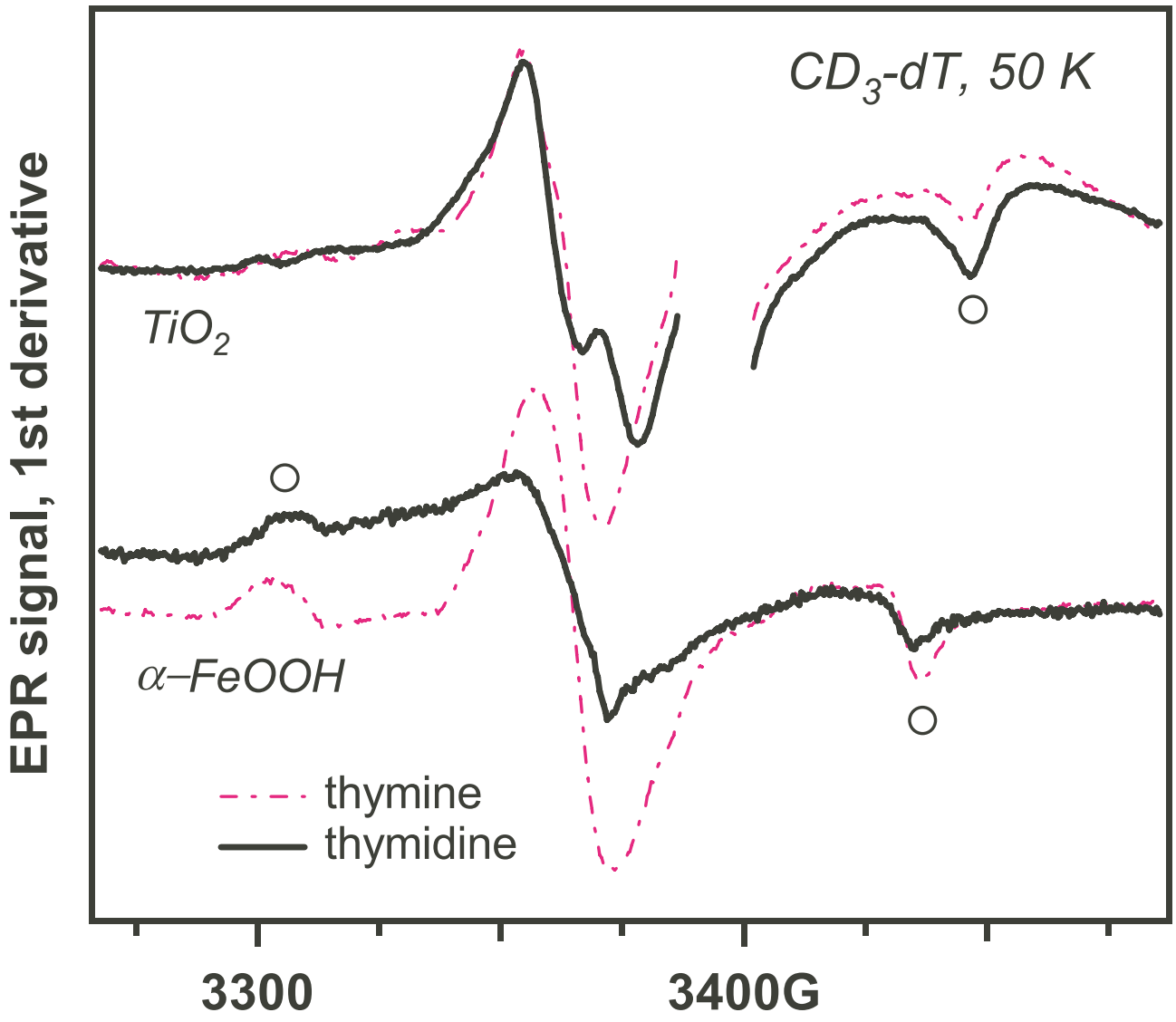
CD3-dT, 50 K
TiO2
α–FeOOH
thymine
thymidine
EPR signal, 1st derivative
3300
3400G

Figure 13S.

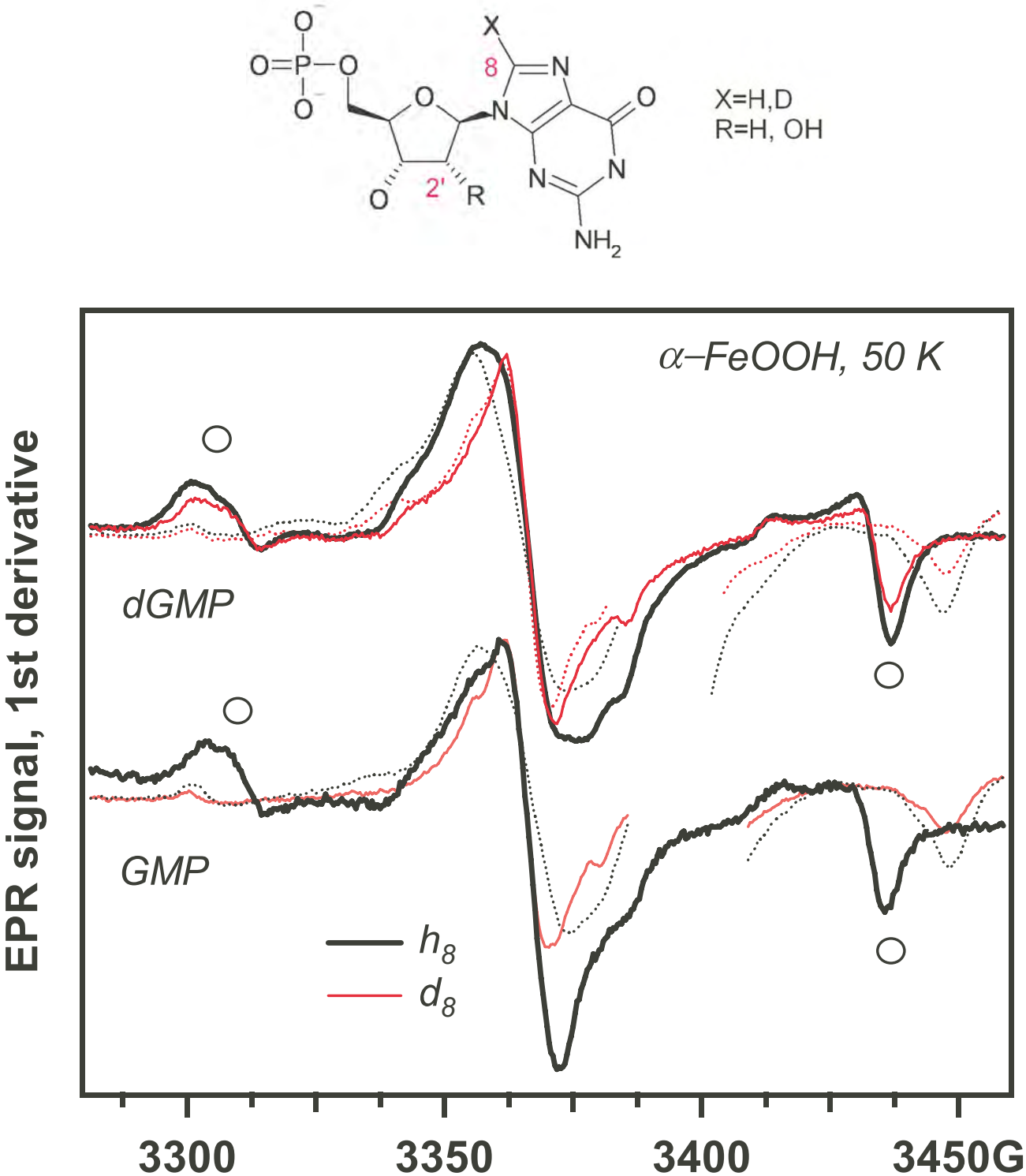

Shkrob et al.

Figure 14S.

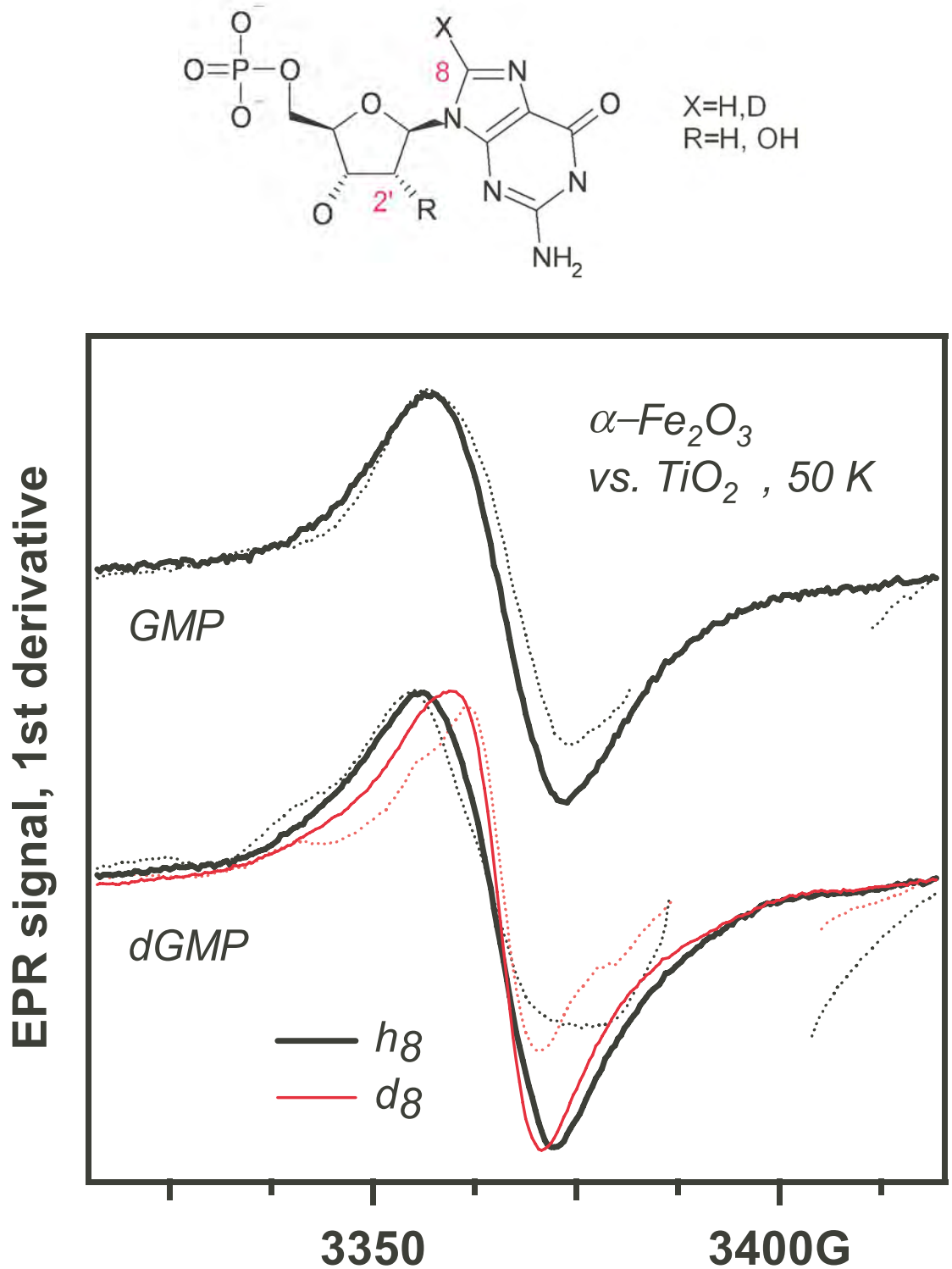

Shkrob et al.